Power Electronic Systems
Laboratory

Proceedings of the 23rd International Symposium on Power Electronics, Electrical Drives, Automation and Motion (SPEEDAM 2016), Anacapri, Capri, Italy, June 22-24, 2016

High-Speed Magnetically Levitated Reaction Wheels for Small Satellites

M. Kaufmann,
A. Tüysüz,
J. W. Kolar,
C. Zwyssig

Eidgenössische Technische Hochschule Zürich
Swiss Federal Institute of Technology Zurich

2016
International Symposium on Power Electronics,
Electrical Drives, Automation and Motion

High-Speed Magnetically Levitated Reaction Wheels for Small Satellites

Maurus Kaufmann, Arda Tüysüz, Johann W. Kolar
Power Electronic Systems Laboratory
Swiss Federal Institute of Technology
Zürich, Switzerland
Email: kaufmann@lem.ee.ethz.ch

Christof Zwyssig
Celeroton Ltd.
Volketswil, Switzerland
Email: christof.zwyssig@celeroton.com

***Abstract*—Mechanical wear and stiction can be eliminated by using magnetic bearings instead of ball bearings in spacecraft reaction wheels. Accordingly, the lifetime of attitude control systems can be increased and a smooth torque can be achieved also at speed zero crossings. Moreover, the microvibration emission of the reaction wheels can be minimized and actively controlled. A further advantage of magnetically levitated reaction wheels is the ability to rotate at speeds higher than the state of the art. High-speed reaction wheels can be made smaller in size; however, they require higher power levels for the same reaction torque. Therefore, this paper analyzes the circulation of energy within different reaction wheels of an attitude control system in order to limit the external power requirement. Moreover, integrated position sensors are used for limiting the axial length of the rotors, thereby further increasing the speed limits that may be resulting from rotor dynamics. A functional demonstrator is built and equipped with two different reaction wheel rotors for initial tests. The electrical machine design and the operation of the magnetically levitated reaction wheel systems are verified experimentally.**

I. Introduction

Reaction wheels are not only the standard solution for attitude control of conventional spacecraft such as telecommunication satellites, but they are also frequently used in smaller (up to a few 100 kg) satellites with demanding attitude control requirements [1], [2]. Most of today's reaction wheels use ball bearings, whose mechanical wear is a significant life-limiting factor [3]. In order to maintain a longer life time, ball bearings are usually operated at speeds below 6 000 r/min, in low-pressure nitrogen atmosphere that prevents oxidation and outgassing of the lubricant.

Using magnetic bearings instead of ball bearings, the hermetic sealing and the friction losses may be omitted since magnetic bearings can run in vacuum. Moreover, a smooth torque can be achieved also at speed zero crossings due to the absence of stiction. Elimination of ball bearings also removes the need for complex friction estimation methods utilized for lubrication condition monitoring [4]. Since mechanical wear is omitted, the life time of the reaction wheel system increases.

A main source of microvibrations in satellites is the forces generated (e.g. by cage vibration or uneven raceways) or transferred (imbalance forces of the rotor) by the ball bearings of reaction wheels. Therefore, a further advantage of using magnetic bearings is the reduction or elimination of microvibrations [5], since the imbalance forces can be omitted by rotating the rotor around its center of mass. Moreover, the microvibration envelop can be adjusted since the bearing force can be actively controlled.

In addition, according to the scaling laws derived in [6], the higher speeds enabled by magnetic bearings can be used for decreasing the size of the reaction wheel considerably for the same angular momentum ratings. Therefore in the same work, a novel, high-speed, magnetically levitated reaction wheel design integrated into a novel dual hetero-/homopolar, slotless, permanent-magnet synchronous motor is presented. On the other hand, the power rating of a high-speed reaction wheel is proportionally higher compared to a low-speed reaction wheel applying the same reaction torque. This may be an advantage if the wheels are also used for energy storage as in Integrated Power and Attitude Control Systems (IPACS). But if the wheels are only used for attitude control, the same fact translates into a larger installed power requirement for the satellite power supply system. This, along with the additional complexity introduced by the position sensing, control, and power amplifiers, is a significant disadvantage of high-speed, magnetically levitated reaction wheels used for attitude control.

Therefore, this paper analyzes ways of reducing the system complexity, size and power requirement of the high-speed magnetically levitated reaction wheel proposed in [6]. Integrated radial position sensors are designed for a more compact and simpler system. In order to limit the external power requirement, an arrangement of two counter-rotating reaction wheels for a single attitude axis is considered instead of a single reaction wheel. In such an arrangement, the total reaction torque to be applied on that axis can be distributed between these two reactions wheels, and power can be circulated between the accelerating and the decelerating wheels, which limits the total external power requirement for a given maneuver. For further reduction of size and complexity, a four-wheel reaction wheel assembly is also studied in which the angular momentum can be controlled in all three axes while limiting the external power requirement.

The current aim of this work is to reach Technology Readiness Level (TRL) 4 according to [7], which is defined as the stage where the basic subsystem components are integrated

978-1-5090-2067-6/16/$31.00 ©2016 IEEE

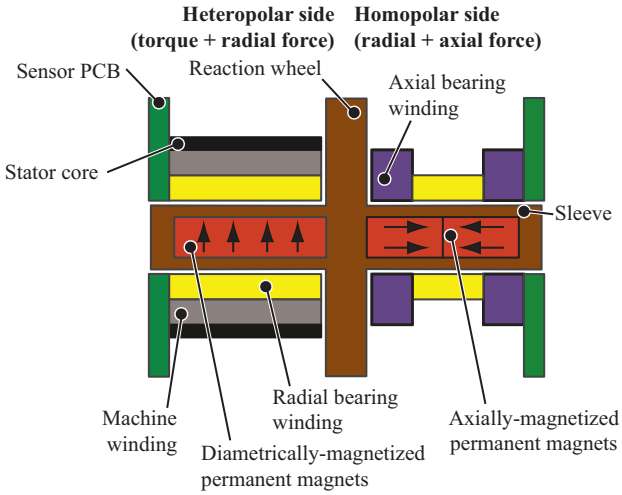

Fig. 1. Cross sectional view of the prototype considered in this work. The machine rotor diameter (permanent magnet + sleeve) is 8 mm on both the homopolar and heteropolar sides. Two different rotors are tested with total axial length, reaction wheel diameter and reaction wheel axial length of 65 mm, 16.5 mm, 22 mm, and 49 mm, 30 mm, 6 mm. Their axial moments of inertia are 806x10^{-9} kg m^2 and 2211x10^{-9} kg m^2, respectively.

to establish a working system in a laboratory environment. To that end, the selection of structural or electronic components is not strictly narrowed down to a limited number of space-qualified devices. Similarly, mechanical stresses that could be expected during launch, or the use of emergency touch-down bearings are not considered.

II. System Description

A. Magnetically Levitated Reaction Wheel

In [8], the use of Lorentz-type magnetic bearings is shown to have very high dynamics due to its slotless structure, and to enable very high (500 000 r/min) rotational speeds owing to low rotor losses. The machine design is further improved in [6], resulting in the machine topology shown in Fig. 1, which is considered in this paper. As opposed to the topology of [8], a dedicated permanent magnet is not required for the axial bearing, and the load (in this case the reaction wheel) is in the axial middle of the rotor. These two modifications lead to better rotor-dynamic performance by increasing the frequency of the first bending mode. A heteropolar self-bearing motor applies torque and radial force on one axial side of the rotor, whereas a homopolar machine topology is used on the other side of the rotor to apply axial and radial forces in order to control all six degrees of freedom actively.

B. Integrated Radial Position Sensors

In the prototype presented in [6], two Printed Circuit Boards (PCBs) containing position sensors are placed on both ends of the rotor as shown in Fig. 1. The radial rotor position is measured on both sides using PCB-integrated eddy-current sensors described in [9]. The axial and angular positions are

Fig. 2. Photograph of the radial position sensor before being rolled and inserted in the stator bore. The sensor is realized as a two-layer flexible printed circuit. Copper thickness is 35 μm and the diameter of via holes is 0.1 mm.

obtained by the measurement of the stray field using Hall-effect sensors [8]. These two PCBs require the machine housing to be axially longer and contribute to the weight overhead, and more importantly, they lead to an axially longer rotor for radial position measurements, which is a very undesired feature from rotor-dynamic perspective.

A hybrid gas-magnetic bearing is presented in [10], where the high load capacity of the gas bearing is utilized for rotor suspension; and a heteropolar Lorentz-type magnetic bearing winding is used for actively damping the system to ensure stable operation over a wide speed range. Since they are used only for damping and not main load support, these magnetic bearings can have a small size, hence they are realized easily as Flexible Printed Circuits (FPCs), which makes the manufacturing simpler. Moreover, as described in detail [10], the bearing windings can be used as eddy-current sensors for measuring radial displacements of the rotor.

In order to omit the rotor's axial length overhead described above, a similar approach is taken in this work. Eddy-current sensors (without damping functionality) are realized as FPC similar to [10], and inserted in the stator bore, inside the magnetic bearing windings on both axial sides of the machine. Consequently, the axial rotor length overhead requirement for the PCB-based sensors is eliminated. Fig. 2 shows the realized FPC-based radial position sensor.

III. Counter-Rotating Reaction Wheels

A. Power Transfer Among Two Reaction Wheels on one Axis

In order to limit the external power P_{ex} requirement, the optimum torque profiles of two identical counter-rotating reaction wheels running on the same axis are investigated such that the reference reaction torque on the considered axis is generated collaboratively ($T_{\mathrm{tot}}(t) = T_1(t) + T_2(t)$) while shifting the power between the two reaction wheels.

At the first stage, the inverter is modeled to be lossless, and only the conduction (Joule) losses are considered in the machines. Energy storage in the common DC-link capacitor of the two drive inverters is not considered for limiting the capacitor size. At the initial time, both wheels are rotating at the same speed, but in reverse directions ($-\omega_0$, ω_0) such that there is no net angular momentum.

The block diagram of the system is given in Fig. 3. J is the moment of inertia of one rotor. The factor $K_{\mathrm{P,cu}}$ relates the

square of the torque T to the copper losses in the windings P_{cu} as

$$K_{\mathrm{P,cu}} := \frac{P_{\mathrm{cu}}}{T^2} = \frac{2}{3} \cdot \frac{R_{\mathrm{m}}}{\Psi_{\mathrm{m}}^2} \,. \tag{1}$$

where R_{m} and Ψ_{m} denote the phase resistance and flux linkage of the machine, respectively. Their numerical values are specified in Table I.

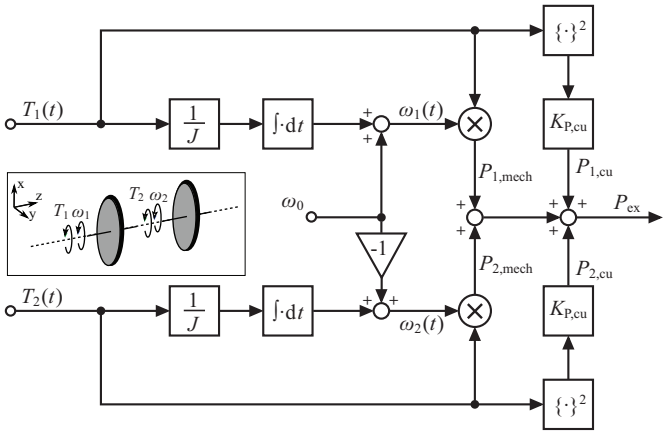

Fig. 3. Block diagram of the two counter-rotating reaction wheels.

TABLE I
VALUES OF THE LUMPED PARAMETERS IN THE THERMAL MODEL AND THE ELECTROMAGNETIC PROPERTIES OF THE ELECTRICAL MACHINE.

C_{wi}	$2.94\,\mathrm{J/°C}$	R_{wi2Fe}	$2.09\,\mathrm{°C/W}$
C_{Fe}	$6.84\,\mathrm{J/°C}$	R_{Fe2Al}	$0.51\,\mathrm{°C/W}$
C_{Al}	$51.2\,\mathrm{J/°C}$	R_{m}	$0.78\,\Omega$
L_{m}	$33\,\mu\mathrm{H}$	Ψ_{m}	$0.69\,\mathrm{mV\,s}$

In order to assess the maximum temperature rise in the machines, a simple lumped-parameter thermal model is used, cf. Fig. 4 and Table I. The model lacks a heat sink, and the heat capacity of the bearing windings is neglected because it is a worst case model focussing on the transient temperature behaviour. C_{wi}, C_{Fe} and C_{Al} denote the heat capacities of the machine windings, the stator core and the aluminium housing, respectively. R_{wi2Fe} is the thermal resistance from the machine windings to the stator core and R_{Fe2Al} from the stator core to the aluminium housing.

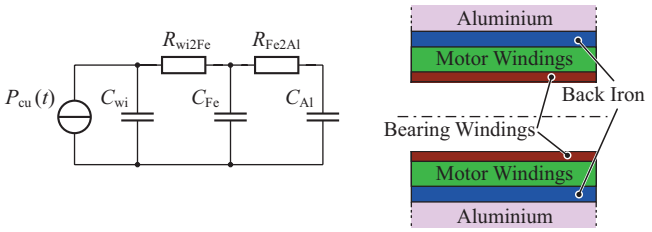

Fig. 4. Lumped parameter thermal model (left) and the approximately cylindrically shaped components of the stator (right).

The torque profiles T_1, T_2 and the initial speed ω_0 of the reaction wheels are optimized numerically to satisfy a given T_{tot}, with the goal of minimizing the copper losses. As boundary conditions, the maximum external power requirement P_{ex} is kept below a defined limit $P_{\mathrm{ex,max}}$ and the maximum speed n_{max} is never exceeded.

The maneuver pattern of a spacecraft is the outcome of mission-specific complex trajectory calculations. In this work, the reference torque T_{tot} is chosen to be constant over a certain active period t_{a} to produce a desired change in angular momentum L_{ref}:

$$L_{\mathrm{ref}} = T_{\mathrm{tot}} \cdot t_{\mathrm{a}} \,. \tag{2}$$

In the following, the maximum external power is limited by $P_{\mathrm{ex,max}} = 5\,\mathrm{W}$. Titanium reaction wheels with a diameter of $30\,\mathrm{mm}$ and an axial moment of inertia of J = 2211x10^{-9} $\mathrm{kg\,m^2}$ are considered. With the theoretical maximum speed of $n_{\mathrm{max}} = 400\,000$ r/min (restricted by the maximum tensile strength of the rotor), the maximum change in angular momentum L_{ref} is $80\,\mathrm{mN\,m\,s}$, which is in the range of commercially available reaction wheels for small satellites [11].

The optimized torque profiles and initial speeds of the two reaction wheels for $L_{\mathrm{ref}} = 80\,\mathrm{mN\,m\,s}$ and an active period $t_{\mathrm{a}} = 16\,\mathrm{s}$ are given in Fig. 5. It can be seen that the reference torque value is satisfied while limiting the external power requirement to 5 W while powers in excess of 70 W are being circulated between the wheels. Here is has to be mentioned that the shown torque profiles are optimized for minimizing the power loss in the machines, which needs to be provided into the system while desaturating the reaction wheels (i.e. bringing the wheel speeds back to the initial values slowly, while different torque sources such as magneto-torquers are being used to stabilize the spacecraft). It would have also been possible to have no input power during maneuver and accelerate one wheel only using the power generated by the decelerating one; however, this would have resulted in higher energy loss which would need to be supplied during desaturation. Fig. 6 depicts the corresponding temperatures of the stator components. The temperature rise is below $40\,\mathrm{°C}$ for this operating point, and the maximum temperature is reached at the end of the active period in the windings.

In Fig. 7, the maximum occurring temperature rise in the motor is investigated in dependency of the active period t_{a} and the desired change of the angular momentum L_{ref}. The dashed blue line indicates $L_{\mathrm{ref}} = 80\,\mathrm{mN\,m\,s}$ with an upper speed boundary of $n_{\mathrm{max}} = 400\,000$ r/min. Operation with $n_{\mathrm{max}} = 200\,000$ r/min, which corresponds to $L_{\mathrm{ref}} = 40\,\mathrm{mN\,m\,s}$ is also studied with the same machine and wheels, and plotted using the dashed red line.

B. Power Transfer Among Four Reaction Wheels

Complete reaction wheel assemblies need to be able to generate an angular momentum in all three Cartesian coordinate axes and to provide redundancy. Therefore, at least four reaction wheels are usually employed. The reaction wheels

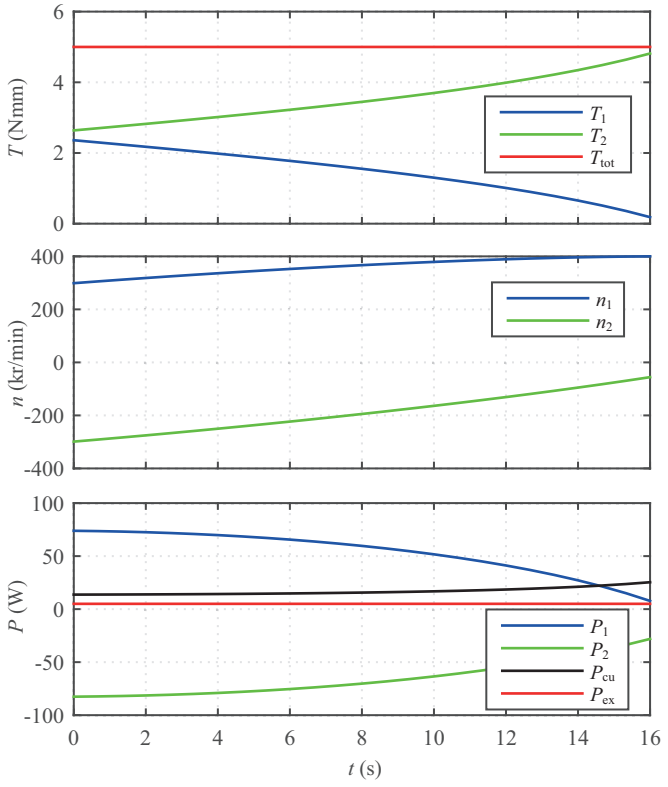

Fig. 5. Reference torque T_{tot} and the torque profiles T_1 and T_2 minimizing the copper losses (top); the corresponding rotational speeds n_1 and n_2 (middle) and the mechanical power consumed by reaction wheel 1 P_1, produced by reaction wheel 2 P_2, the copper losses P_{cu} and the external power P_{ex} fed to the two wheels (bottom). Rotational speeds in kr/min are obtained as $n = \omega \frac{3}{100\pi}$, where ω is the rotational speed in rad/s.

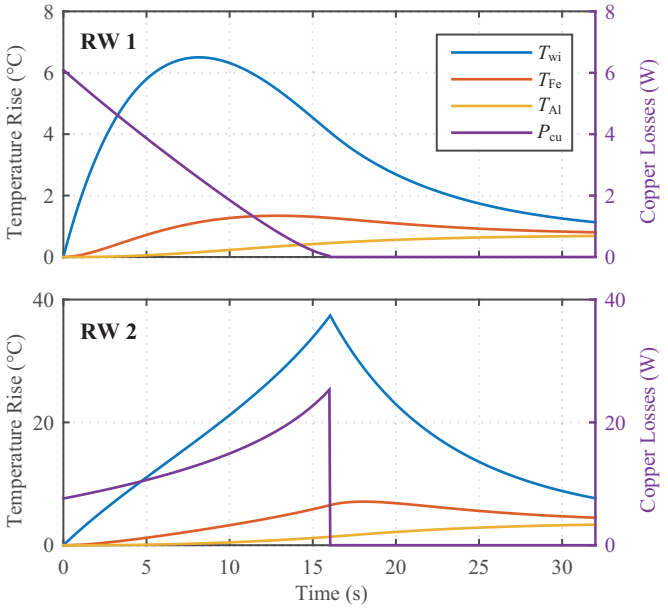

Fig. 6. Copper losses P_{cu} and temperature of the windings T_{wi}, the back iron T_{Fe} and the aluminium housing T_{Al} over time of reaction wheel 1 (top) and reaction wheel 2 (bottom) for the torque profile depicted in Fig. 5.

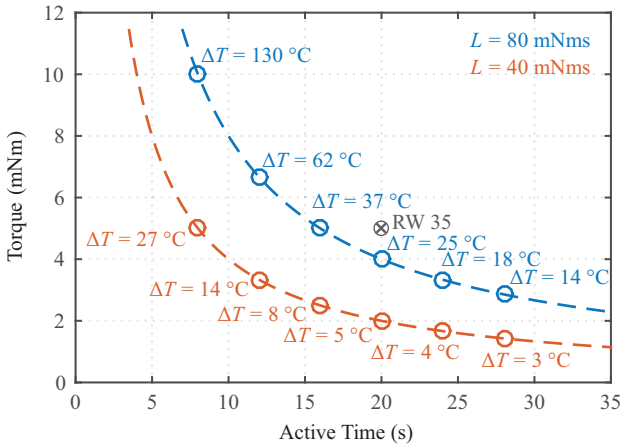

Fig. 7. Maximum rises of the temperature ΔT in the windings for different active periods t_{a} and two different values of angular momentum change. The black point labeled by RW 35 represents a commercially available reaction wheel with a nominal torque of $5\,\mathrm{mN\,m}$ and an angular momentum of $0.1\,\mathrm{N\,m\,s}$ [11]. It is located in the vicinity of combinations of T and t_{a} with viable temperature rises assuming a worst case ambient temperature of $60\,^{\circ}\mathrm{C}$.

can be arranged in different geometric ways, e.g. pyramidal or tetrahedral configuration [12]. Considering, high-speed magnetically levitated reaction wheels, as long as all four reaction wheels are working properly, the degree of freedom arising from the redundancy can be used to circulate power among the reaction wheels in order to limit the external power.

As an example, Fig. 8 shows the optimum torque profiles and initial speeds that minimize the copper losses P_{cu} in a pyramidal four-wheel configuration, where the same machine and reaction wheels are considered as above, and the desired angular momentum changes in x, y and z axes are 30, 50 and 40 $\mathrm{mN\,m\,s}$, respectively. As it can be seen, through an optimum torque profile, the external power requirement can be kept to a minimum while achieving the reference torques in all three axes. These results verify that, along with all the other benefits of using magnetically levitated reaction wheels, there is a significant room for weight and complexity reduction at healthy operating conditions as long as reduced angular momentum control or increased external power can be accepted under fault conditions - which may be the case for certain missions.

IV. Experimental Verification

The operation of the FPC position sensor is verified by standstill measurements where the rotor is held still at a given position, and the displacement is measured in x- and y-directions using the FPC position sensor as well as an external optical sensor for reference. As shown in Fig. 9(a), the sensor output is very linear, and there is a rather small cross coupling between the x- and y-directions, especially for displacements smaller than ± 250 μm. Fig. 9(b) verifies the repeatability and low-noise characteristics of the sensor.

The machine is operated with two different reaction wheels with diameters of 30 mm and 16.5 mm and axial moments

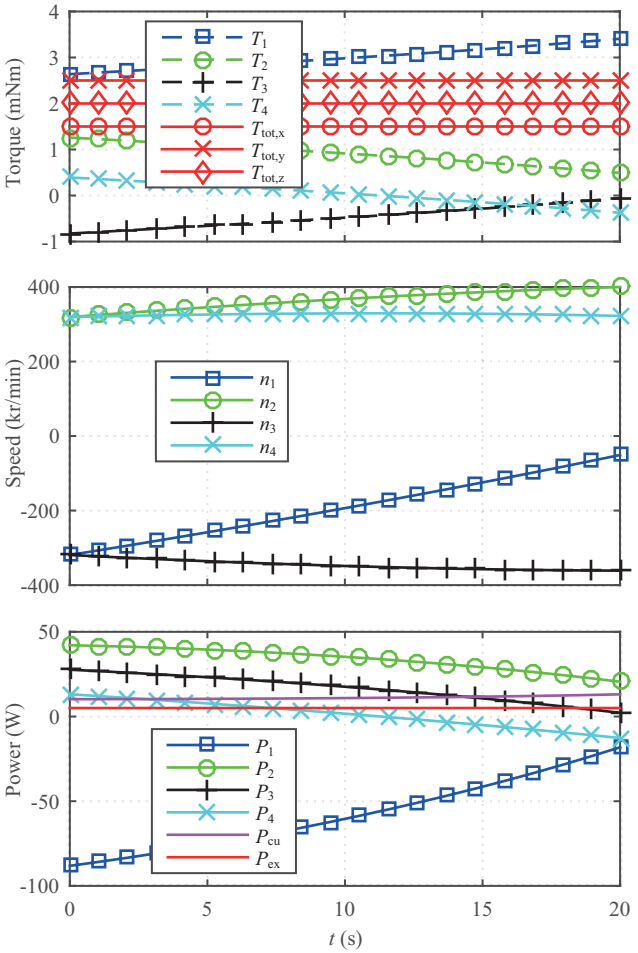

Fig. 8. Reference torques $T_{\mathrm{tot,x/y/z}}$ in the three Cartesian coordinate axes and the torque profiles T_1–T_4 minimizing the copper losses (top); the corresponding rotational speeds n_1–n_4 (middle) and the mechanical powers consumed or produced by the reaction wheels P_1–P_4, the copper losses P_{cu} and the external power P_{ex} fed to the four wheels (bottom). The active period is 20 s and . The maximum speed is $n_{\max} = 400\,000$ r/min and the allowed external power consumption is $P_{\mathrm{ex,max}} = 5\,\mathrm{W}$.

of inertia of 2211x10^{-9} kg m^2 and 806x10^{-9} kg m^2. Their no-load losses are measured in vacuum and in air, and plotted in Fig. 10. It can be seen that the major part of the total losses is the air-friction losses, and it is the main source of mismatch between the calculated and measured loss values. This, however, is not investigated further since in the targeted space applications, the machines may run in vacuum due magnetic levitation.

Finally, Fig. 11 depicts the measured rotor displacements and the bearing currents at both the homopolar and heteropolar sides for the reaction wheel with 30 mm diameter when the operating speed is 90 kr/min. The highest measured displacement is less than 20 μm. The larger orbit on the homopolar side results from higher unbalance.

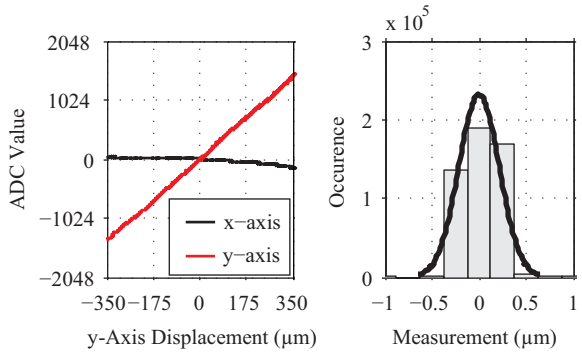

Fig. 9. (Left) Displacement measurement at standstill using the flexible printed circuit position sensor in the heteropolar side. Vertical axis shows the sampled values by the Analog-to-Digital Converter (ADC) after the filtering and amplitude demodulation steps, which are described in [10]. The rotor is held using a mechanical fixture and displaced only in the y-direction (x-direction displacement is zero). The reference measurement is obtained by an external optical displacement sensor (Keyence LK-H022). (Right) Histogram of the sensor measurement in y-direction at zero displacement.

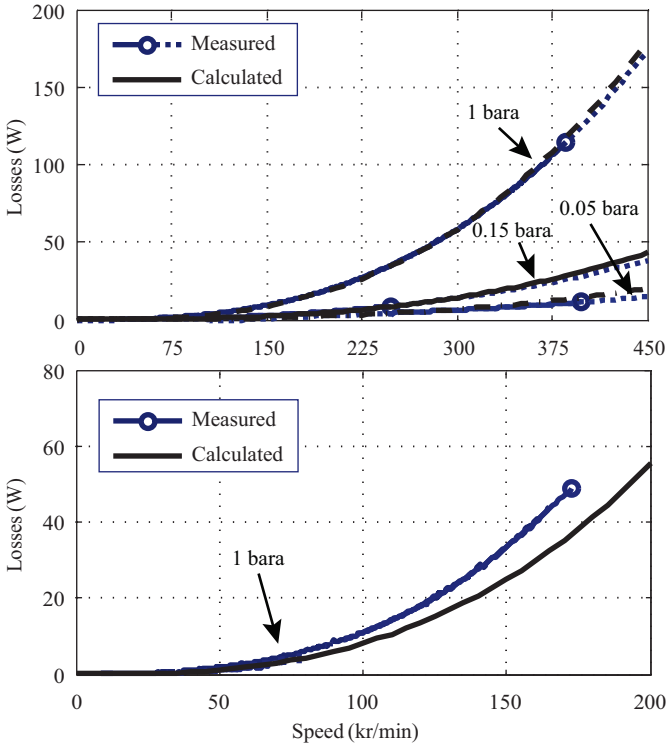

Fig. 10. Calculated and measured losses of the machine when driving reaction wheels with 16.5 mm diameter (top), and 30 mm (bottom). Measurements with the smaller wheel are carried out under 1, 0.15 and 0.05 bar absolute (bara) air pressures. Losses are calculated based on the no-load deceleration speed profiles and the known inertia of the rotors. Circles denote the speeds that the deceleration tests started from, and the dashed lines show the extrapolation of the losses towards higher speeds.

V. Conclusion

Using magnetic bearings instead of ball bearings for suspending the reaction wheels used in small spacecraft attitude control systems, the mechanical wear and stiction can be

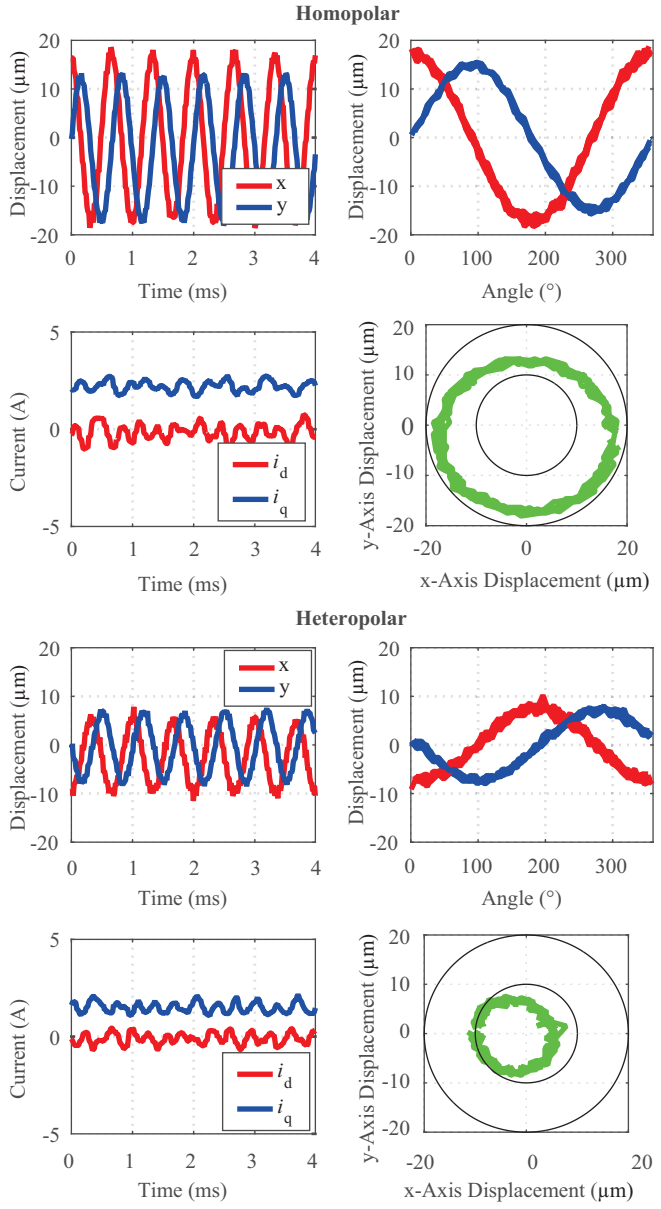

Fig. 11. Rotor displacements and bearing currents in the heteropolar and homopolar sides for the the 30 mm reaction wheel rotor at the rotational speed of 90 kr/min.

eliminated. Accordingly, the reliability of the attitude control system can be increased and a smooth torque can be achieved also at speed zero crossings. Furthermore, the hermetic sealing and complex lubrication monitoring methods may be omitted, reducing the size and complexity of the attitude control system. Additionally, the microvibration emission of the attitude control system can be actively controlled and limited.

A further advantage of magnetically levitated reaction wheels is the ability to rotate at speeds higher than the state of the art systems, which are currently limited to around 6 000 r/min. This gives the spacecraft designers a further degree of freedom in system optimization. Even though the high-speed reaction wheels can be made smaller in size, they require higher power levels for the same reaction torque. Therefore, this paper analyzes the circulation of energy within different reaction wheels of the attitude control system in order to limit the external power requirement. Finally, integrated position sensors are used for limiting the axial length of the rotors, thereby further increasing the speed limits that may be resulting from rotor dynamics.

A functional demonstrator is built and equipped with two different reaction wheels for initial tests. The machine design and the operation of the magnetically levitated reaction wheel systems are verified experimentally.

References

[1] M. Scharfe, T. Roschke, E. Bindl, D. Blonski, and R. Seiler, "The challenges of miniaturisation for a magnetic bearing wheel," in *Proceedings of the 9th European Space Mechanisms and Tribology Symposium*, 2001.

[2] B. Xiao, M. Huo, X. Yang, and Y. Zhang, "Fault-tolerant attitude stabilization for satellites without rate sensor," *IEEE Transactions on Industrial Electronics*, vol. 62, no. 11, pp. 7191–7202, April 2015.

[3] S. Marble and D. Tow, "Bearing health monitoring and life extension in satellite momentum/reaction wheels," in *Proceedings of the IEEE Aerospace Conference*, 2006.

[4] M.-C. Chou and C.-M. Liaw, "Dynamic control and diagnostic friction estimation for an SPMSM-driven satellite reaction wheel," *IEEE Transactions on Industrial Electronics*, vol. 58, no. 10, 2011.

[5] State Secretariat for Education, Research and Innovation and Swiss Space Office. (2013) Swiss space implementation plan within education, research and innovation for 2014-2023. [Online]. Available: www.sbfi.admin.ch

[6] C. Zwyssig, T. Baumgartner, and J. W. Kolar, "High-speed magnetically levitated reaction wheel demonstrator," in *Proceedings of the International Power Electronics Conference (IPEC - ECCE Asia)*, May 2014, pp. 1707–1714.

[7] European Space Agency. (2016) Future missions office website. [Online]. Available: http://sci.esa.int/future-missions-office

[8] T. Baumgartner, R. M. Burkart, and J. W. Kolar, "Analysis and design of a 300-W 500 000-r/min slotless self-bearing permanent-magnet motor," *IEEE Transactions on Industrial Electronics*, vol. 61, no. 8, pp. 4326–4336, Aug 2014.

[9] A. Muesing, C. Zingerli, P. Imoberdorf, and J. W. Kolar, "PEEC-based numerical optimization of compact radial position sensors for active magnetic bearings," in *Proceedings of the 5th International Conference on Integrated Power Systems (CIPS)*, March 2008, pp. 1–5.

[10] A. Looser and J. W. Kolar, "An active magnetic damper concept for stabilization of gas bearings in high-speed permanent-magnet machines," *IEEE Transactions on Industrial Electronics*, vol. 61, no. 6, pp. 3089–3098, June 2014.

[11] Astro- und Feinwerktechnik Adlershof GmbH. Reaction wheel RW 35 for nano and micro satellites (data sheet). [Online]. Available: http://www.astrofein.com

[12] I. Kök, "Comparison and analysis of attitude control systems of a satellite using reaction wheel actuators," Master's thesis, University of Würzburg and Lulea University of Technology, 2012.